

Phase Diagram of a Nearly Isorefractive Polyolefin Blend

Howard Wang,^{*,†} Katsumi Shimizu,[†] Erik K. Hobbie,[†] Zhi-Gang Wang,^{†,‡}
J. Carson Meredith,[†] Alamgir Karim,[†] Eric J. Amis,[†] Benjamin S. Hsiao,[‡]
Eric T. Hsieh,[§] and Charles C. Han^{*,†}

Polymers Division, National Institute of Standards and Technology, Gaithersburg, Maryland 20899; Department of Chemistry, State University of New York, Stony Brook, New York 11794; and Chevron Phillips Chemical Company, Bartlesville, Oklahoma 74004

Received May 23, 2001; Revised Manuscript Received October 26, 2001

ABSTRACT: The phase diagram of coexisting liquid–liquid phase separation (LLPS) and crystallization in nearly isorefractive blends of statistical ethylene/hexane (PEH) and ethylene/butene (PEB) copolymers has been investigated. A variety of techniques that exploit crystallization-induced contrast, such as diffuse light scattering, small-angle light scattering, light transmission, atomic force microscopy, and differential scanning calorimetry, are used to identify the LLPS boundary, which is found to exhibit an upper critical solution temperature of 146 °C. The composition dependence of the LLPS boundary follows the prediction of Flory–Huggins theory for binary polymer mixtures. The equilibrium melting temperature of the blends decreases with increasing PEB concentration in the miscible phase, whereas it remains relatively constant at 127 °C within the LLPS coexistence region. Measurements of the LLPS boundary can be complicated by heterogeneity in the polymer microstructure.

Introduction

Olefin polymers are the most widely used materials in the plastics industry today. To optimize their properties and processibility, blending is often used.^{1,2} This is particularly important for the metallocene-catalyst based polyolefins. By altering certain shear-thinning and strain-hardening characteristics, blending can enhance the processibility of the material. This is in addition to any property enhancement or modification already formulated into the blending or alloying process. With all these requirements, the specific compounding and manufacturing processes become complicated and difficult to control if the fundamental physical principles are not understood. In the case of polyolefin blends, the mixtures can undergo both liquid–liquid phase separation (LLPS) and crystallization, complicating the blend morphology and thus limiting control of the properties of the final product. To understand the driving forces that dictate the morphology of the blend, it is critical to have a quantitative measure of the phase diagram. In recent years, much effort has been directed toward determining and understanding macroscopic LLPS in blends of ethylene-based polyolefins with various microstructures.^{3,4}

Previous studies on LLPS in polyolefin blends can be divided into two main categories: crystallization-induced contrast^{1,5–10} and scattering on both model polymers^{11–20} and mixtures of metallocene-catalyst based copolymer with model polymers.²¹ For the former, studies have focused mostly on blends of linear polyethylene (LPE) and low-density polyethylene (LDPE) or linear low-density polyethylene (LLDPE) and relied mostly on microscopy to determine the crystal morphology in previously phase-separated liquid domains. Because techniques such as transmission electron micros-

copy (TEM) are often very tedious, these measurements result in a coarse morphological mapping rather than an accurate determination of the LLPS boundary.^{8–10} For small-angle neutron scattering (SANS)^{12–15} and nuclear reaction analysis,^{17,18} the contrast between the two polymers is introduced by deuterium labeling of one of the components. If the difference in polymer microstructure is large enough to give rise to significant optical contrast, then light scattering can be used.¹⁵ From the scattering studies, the interactions between model polymers with different densities of methyl or ethyl branches are relatively well understood. Although highly sensitive, neutron scattering from deuterium-labeled polymers is not desirable for practical applications, since such chemical modification can often be expensive and can also induce changes in the already subtle olefin interactions.¹⁴ On the other hand, light-scattering studies of polyolefin blends are often hindered by the small refractive index difference, and hence the small optical contrast, between the polymers.

In this article, we report a convenient and sensitive route for measuring the phase diagram of a blend of two short side-chain branched polyethylenes. These metallocene-synthesized random copolymers have relatively narrow molecular-mass and branching-density distributions, bridging the gap between heterogeneous, multi-site-catalyst-synthesized polymers, and model, anionically polymerized polymers. Due to microstructural similarities, the two components have almost identical refractive indices, and thus, conventional methods of determining the liquid–liquid phase boundary (such as cloud-point measurements) are not readily applicable. In the present study, a new approach that employs indirect methods based on diffuse light scattering has been developed. This approach can be applied to any polymer blend in which one of the components is more crystallizable.

Materials and Experiment

The polymers used in this study are statistical copolymers of ethylene/hexene (PEH) and ethylene/butene (PEB), and are

* To whom correspondence should be addressed. E-mail: H.W., hao.wang@nist.gov; C.C.H., charles.han@nist.gov.

[†] National Institute of Standards and Technology.

[‡] State University of New York, Stony Brook.

[§] Chevron Phillips Chemical Company.

Table 1. Characteristics of PEH and PEB

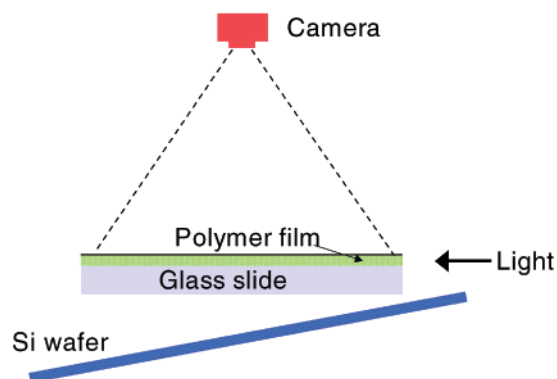
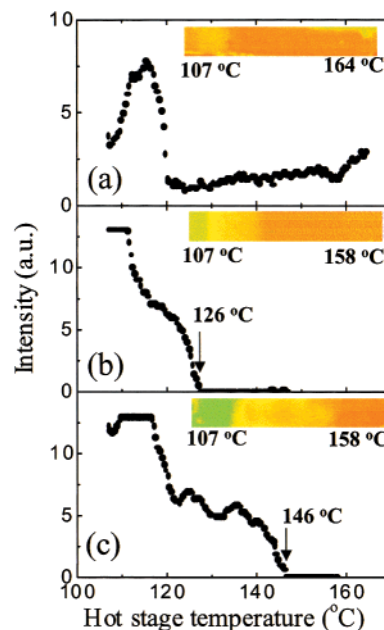
polymer	M_w (kg/mol)	ρ_m (g/cm ³)	SCD (per 10 ³ C)	T_m (°C)
PEH	112	0.922	9	120
PEB	70	0.875	77	48

both synthesized with metallocene catalysts.²² The characteristics of the two polymers, including mass-averaged molecular mass (M_w), mass density (ρ_m) of as-received polymers, and side chain density (SCD, in units of per 1000 backbone carbon atoms), as well as the melting temperature, T_m , are listed in Table 1. The T_m 's of PEH and PEB were measured using a Perkin-Elmer differential scanning calorimeter (DSC7²²) and were defined as the endothermic peak temperatures at a heating rate of 10 °C/min. PEH is the more readily crystallizable component in the blend. Blends of varying composition were prepared by coprecipitating from a hot xylene solution (ca. 100 °C) into cold methanol (ca. 0 °C). After filtering, the polymers were dried in air for a day and further dried in a vacuum oven at 100 °C for 3 days. The mixtures were hot-pressed between two glass plates at 160 ± 0.5 °C to form films of ca. 20 μm thickness and then quenched to room temperature in air. The blends with $x\%$ PEH mass fraction are denoted as H x (e.g. H50, H20, etc.).

A film of premixed blend was kept in the melt at 160 ± 1 °C for 5 min, and then transferred quickly to a temperature gradient hot stage²³ with temperatures ranging from 80 ± 1.5 to 180 ± 0.5 °C over a 40 mm span. Temperatures on the sample were calculated based on a linear relation to the position on the hot stage. After 60 min on the stage, the sample was quenched to room temperature by removing it from the hot stage and letting it cool in air naturally. Throughout this paper, "quench to room temperature" refers to this same process. Crystallization during cooling creates contrast between the different phase morphologies that are present just prior to the final quench to room temperature. The crystalline morphology was characterized using diffuse and small-angle light scattering, light transmission, and atomic force microscopy. The diffuse light scattering (DLS) was the primary technique for identifying the LLPS temperature (T_s) at various blend compositions, whereas other techniques served as a confirmation or consistency check of the DLS results.

For DLS, an intense incoherent light source from an optical fiber was directed into the slide parallel to the polymer film from the edge of the glass substrate, and the images of the samples were recorded using a high-resolution CCD camera (Princeton Instruments, model RTE/CCD-1300Y)²² facing the sample surface (Figure 1). The measured intensity was thus due to the scattering of the light propagating in the slide by the sample at a given position to the direction at 90°. As an important part of this measurement, the background light was suppressed by placing a highly reflective silicon wafer behind the sample, which reflected the stray light away from the camera.

For the light-transmission measurements, a He-Ne laser with a wavelength of 633 nm was directed through the sample and the intensity of the transmitted light was measured using a power meter. The transmission was measured at points of equal spacing along the strip, corresponding to different temperatures on the gradient hot stage, and normalized with that measured for the bare cover slip and glass slide. For the depolarized small-angle light-scattering (SALS) measurements, the same laser light source was used. Linearly polarized laser light was scattered by the sample and then filtered with an analyzer polarized perpendicular (H_\perp) to the polarization direction of the incident light.²⁴ The scattering pattern was imaged on a screen behind the analyzer and recorded with the high-resolution CCD camera, with a q range spanning from 0.05 to 1.8 μm^{-1} . The equilibrium melting temperatures of the blends were measured with differential scanning calorimetry (DSC) using the Hoffman-Weeks approach.²⁵ Atomic force microscopy (AFM) was also used to verify the phase morphology within different regions of the phase diagram. The sample preparation for AFM measurements differed from the previous descriptions only at the first step; blends were melt-pressed

**Figure 1.** Schematic illustration of the diffuse light-scattering measurement.**Figure 2.** Intensity of scattered light as measured from the 2-D images of the polymer strips (see insets, where the false color was used to indicate the intensity from high to low in the order of green to yellow to red.) after the sample has been annealed on a temperature gradient hot stage and quenched to room temperature for (a) PEH, (b) H20, and (c) H50. The horizontal axis indicates the temperature on the gradient hot stage. The temperatures for liquid-liquid phase separation are 126 and 146 °C for H20 and H50, respectively, as indicated by arrows.

between two clean silicon wafers, and one wafer was removed after quenching to room temperature. A Digital Instrument Dimension 3100 microscope²² was used for this study. The measurements were carried out in tapping mode. Both height and phase modes were recorded, with the former revealing topological information and the latter providing contrast in mechanical properties that differentiate crystalline from amorphous phases.

Results and Discussion

Figure 2 shows the DLS scattering patterns and corresponding averaged intensity for each hot stage temperature for (a) PEH, (b) H20, and (c) H50. The pattern of PEH shows a bright region at around 115 °C. Both H20 and H50 blends show three distinct regions: a very bright region at low temperature, an intermediate bright region at higher temperatures, and dark region at even higher temperatures. Note that the intermediate region of H20 has a different width from

that of H50. These observations are quantified by averaging the intensity along a direction perpendicular to the temperature gradient axis. The intensity profile of PEH has a single peak at a temperature between 110 and 120 °C. At temperatures higher than 120 °C, the intensity increases gradually. For both blends, the intensity is high at low temperatures (the dynamic range of the camera was purposely saturated to give the best sensitivity over the region of interest) and then decreases to a plateau before falling to zero at higher temperatures. The transition to zero intensity is found at 146 °C for H50 and 126 °C for H20. Other observed blends fall into two categories; those similar to H20 and H50, such as H30, H40, H60, and H70, and those similar to PEH, such as H10 and H90. The H80 blend gave ambiguous results.

In the diffuse scattering measurements, the degree of brightness indicates the degree of inhomogeneity, corresponding to either regions of crystalline order over length scales comparable to the wavelength of the laser light or coexisting phases with different average crystallinity. Upon transferring of the sample from the melt at 160 °C to the temperature gradient hot stage, PEH, both pure and in blends, crystallizes rapidly at the low-temperature end, forming small crystals that scatter light only weakly. At temperatures between 100 and 120 °C, crystal growth is relatively slow, implying that large crystals can form, giving rise to strong light scattering. For PEH at temperatures higher than ca. 120 °C, little or no crystallization occurs on the hot stage. Upon cooling to room temperature, polymers held at higher temperature may remain longer in the temperature range for crystallization, and the subsequent growth of larger crystallites might explain the intensity upturn for PEH previously held at higher temperatures. For the H20 and H50 blends, the low-temperature features are similar to PEH. In the melt, however, liquid–liquid phase separation can occur. Branched polyethylene blends usually exhibit upper-critical-solution-temperature (UCST) phase behavior,^{13,14,16} and it is expected that the melt will be homogeneous above the phase boundary. Upon rapid cooling from a homogeneous melt, large crystallites cannot form because the lightly branched PEH chains are diluted by the highly branched PEB chains, which themselves can only grow small crystals due to the segregation of the side chain to the surface of the crystallite. The morphology is uniformly distributed fine crystals, as shown below (Figure 6c), and little light is scattered. Once LLPS domains have formed, however, crystals can grow to larger size and/or multiple crystallites can nucleate within the PEH-rich phase upon cooling to room temperature, and the average crystallinity differs in PEH-rich and PEH-poor phases, with both of these factors increasing the intensity of the scattered light. The latter contribution causes a higher scattering intensity from the phase-separated blend than from the pure PEH at the same temperature on the hot stage. Therefore the crossover from regions of finite to little scattering indicates the temperature of liquid–liquid phase separation, denoted as T_s . From Figure 2, parts b and c, T_s is 126 °C for H20 and 146 °C for H50, respectively, reflecting the composition dependence of the LLPS temperature.

Figure 3 shows light transmission as a function of gradient hot stage temperature for PEH and H50, which exhibit very different characteristics. Transmission measurements of PEH show a dip at around 115 °C,

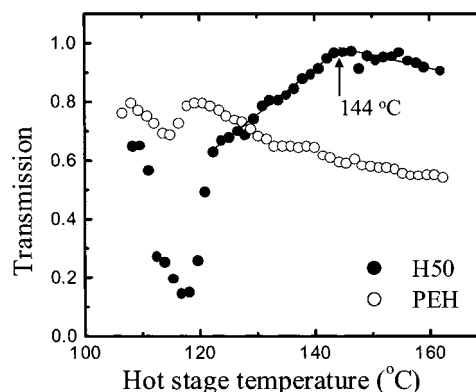


Figure 3. Light transmission for PEH and H50 as a function of the temperature on the hot stage. A single dip around 115 °C is observed for PEH, whereas for H50, a deep dip is followed by a region of linear increase at temperatures between 123 and 144 °C. The latter is identified as the liquid–liquid phase separation temperature for this blend.

followed by a gradual decrease at higher temperatures. These features correspond well with the diffuse scattering measurements, since regions of higher scattering give smaller transmission. For H50, there are three distinct temperature regions: (1) a steep depression at low temperatures (around 115 °C) corresponding to simultaneous isothermal crystallization and phase-separation on the gradient hot stage, (2) a linearly increasing regime (from 123 to 144 °C) corresponding to phase separation in the melt prior to cooling, and (3) a plateau regime at high temperatures (>144 °C) corresponding to an initially homogeneous melt state. In region 1, isothermally grown crystals can have lamellae spanning many micrometers, and their coexistence with LLPS can introduce a high degree of inhomogeneity, thus scattering light strongly. In region 3, quenching from a homogeneous mixture leads to the growth of fine fibrous crystals whose dimension (ca. 50 nm, as will be discussed later) is much smaller than the wavelength of the laser light (633 nm). In region 2, below the transition temperature at ca. 144 °C, a linear increase of transmission with temperature might indicate decreasing optical contrast between the two coexisting phases, due to a smaller difference in the crystallizable PEH composition, or simply less and smaller crystallites in the PEH-rich phase due to higher PEB composition and a larger dilution effect.

To demonstrate the validity of the above picture, SALS measurements were performed on a sample with a slightly different thermal history. A H50 blend was initially quenched from a homogeneous melt at 160 ± 0.5 °C to room temperature, then directly transferred to the temperature gradient hot stage, annealed for 60 min, and quenched to room temperature. Figure 4 shows H_v light-scattering patterns taken at room temperature. The temperature under each image indicates the corresponding temperature on the hot stage. The total uncertainty is ± 2 °C, due to temperature fluctuations on the hot stage as well as the finite size of the laser beam during the measurement. A symmetric four-lobed pattern, indicative of a spherulitic morphology, is observed at most temperatures. On the low-temperature end of the gradient hot stage, the spherulites grown during the quench from the melt (homogeneous) state are preserved and annealed. At 118 and 121 °C, however, no discernible four-lobe pattern is apparent. In this temperature regime, small crystals, which grew

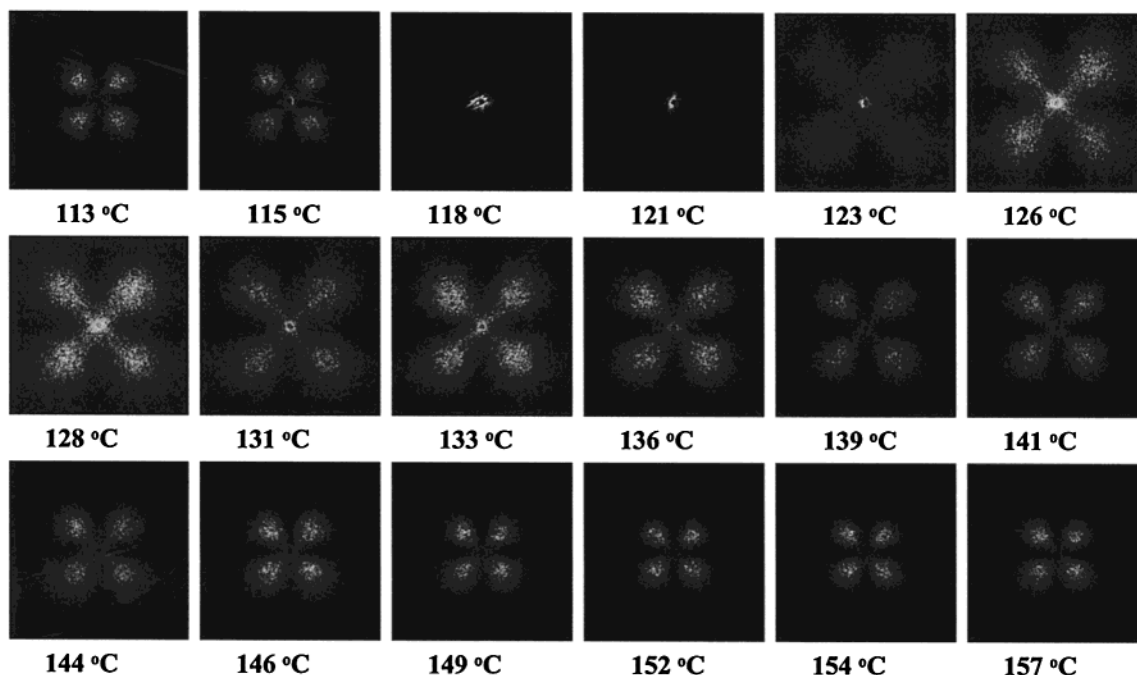


Figure 4. H_v patterns of SALS from H50 annealed at various temperatures on the temperature gradient hot stage for 60 min and subsequently quenched to room temperature. The overall q range of the scattering pattern is 0.05 to $1.8 \mu\text{m}^{-1}$.

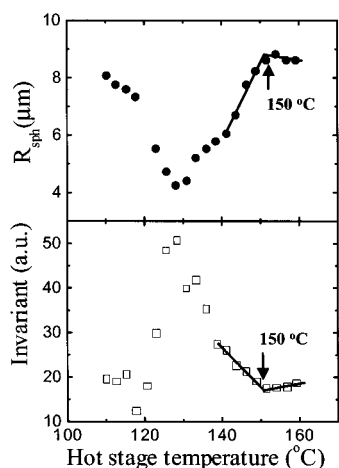


Figure 5. Average radius of the spherulites and the scattering invariant as calculated from the H_v scattering patterns shown in Figure 4 for H50. For both quantities, a transition around $150 \text{ }^\circ\text{C}$ is observed.

during quenching, melt, and LLPS can occur. Competing phase separation and crystallization prohibit the growth of well-ordered spherulitic symmetry. At higher temperatures, the blend is molten on the hot stage, and crystallization only occurs upon cooling to room temperature. The crystal morphology is therefore affected by the morphology of LLPS, the domain size and composition of which depend strongly on quench depth for LLPS. This interference is partly reflected through the continuously varying H_v scattering patterns. At even higher temperatures, the polymer blend is a homogeneous melt. When this is cooled to room temperature, the growth of spherulites is thus less sensitive to the initial temperature on the hot stage.

The H_v scattering patterns can be quantified by q_{max} , the wave vector of the intensity maximum along lines at 45° to the polarization axes, which gives the mean spherulite dimension, $R_{\text{sph}} = 4.08/q_{\text{max}}$,²⁴ and through the scattering invariant, $Q = \int_{q_1}^{q_2} I(q)q^2 dq$, where q_1

and q_2 represent the detector limits. Figure 5 shows (a) the average spherulite radius and (b) the scattering invariant for H50 as a function of the hot stage temperature. Both quantities show an abrupt change in slope at high temperature as indicated by an arrow, suggesting a change from a LLPS state to a homogeneous state prior to crystallization. From these plots, the transition temperature is seen to be around $150 \text{ }^\circ\text{C}$.

The scattering techniques are complemented by real space observations. Figure 6 shows the morphology of H50 along the strip measured with AFM after annealing at (a) 114 ± 1 , (b) 135 ± 1 , and (c) $160 \pm 0.5 \text{ }^\circ\text{C}$ on the hot stage and quenching to room temperature. These phase contrast images correspond to three different regions of interest: (a) isothermal crystallization on the hot stage, (b) crystallization during cooling in a phase-separated state, and (c) crystallization during cooling from an initially homogeneous melt. The morphologies in these three conditions are very different. In part a, stacking of lamellae of many microns near the center of a spherulite is clearly visible. In part b, crystalline aggregates, two of them being pointed at by the arrows, are separated, indicative of the inhomogeneous liquid medium in which they grow, while in part c, fibrous crystals of ca. 50 nm wide are uniformly distributed, suggesting crystal growth in a homogeneous liquid medium.

Calorimetry was used to determine the equilibrium melting temperature of pure PEH and PEH/PEB blends. Selected DSC endotherms for H90 after isothermal crystallization at temperatures of 112, 114, 116, and $118 \text{ }^\circ\text{C}$ for 20, 45, 60, and 120 min, respectively, and subsequently scanned from the isothermal temperature at a rate of $10 \text{ }^\circ\text{C}/\text{min}$, are shown in Figure 7. The peak endotherm temperature, T_m , increases, whereas the heat of melting decreases with increasing crystallization temperature, T_c . The inset of Figure 7 shows T_m as a function of T_c . The intersection of a linear, high- T_c extrapolation of $T_m(T_c)$ and the line $T_m = T_c$ gives the equilibrium melting temperature,²⁵ $T_m^0 = 135 \pm 2 \text{ }^\circ\text{C}$

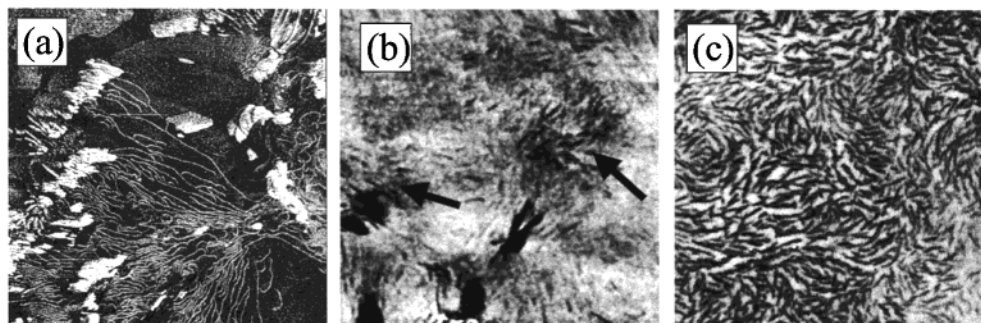


Figure 6. AFM images showing morphologies corresponding to different thermal histories: (a) isothermal crystallization at 114 °C, 10 $\mu\text{m} \times 10 \mu\text{m}$; (b) crystals grown during quenching from segregated liquid phases at 135 °C, 6 $\mu\text{m} \times 6 \mu\text{m}$; (c) crystals grown during cooling from a homogeneous melt at 160 °C, 4 $\mu\text{m} \times 4 \mu\text{m}$.

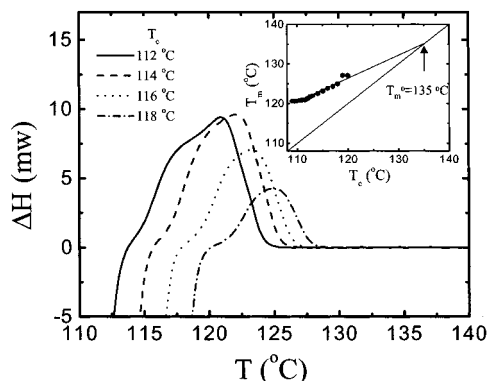


Figure 7. DSC scans on H90 after isothermal crystallization at 112 (solid), 114 (dash), 116 (dot), and 118 °C (dash-dot). The peak in the endotherm, T_m , increases with the crystallization temperature, T_c , and the inset shows T_m as a function of T_c . The intersection with the line $T_m = T_c$ gives an equilibrium melting temperature of 135 °C for H90.

for H90, with the uncertainty given by a linear regression. At low crystallization temperatures, where the size of the crystallites is relatively constant (due to the finite cooling rate compared to the rapid crystallization kinetics), T_m is nearly constant. At the two highest isothermal temperatures, the melting temperature is noticeably larger than the linear extrapolation. This is common for all the blends and the PEH and is probably due to lamellar thickening during the isothermal crystallization. In evaluating T_m^0 , data that obviously deviated from the linear relation have been omitted. Linear regression over a limited regime possibly causes an overestimate of T_m^0 of the PEH, raising the question of the meaningfulness of T_m^0 in statistical copolymers. However, this quantity can be a useful reference for considering the driving force for crystallization.

The LLPS diagram of the PEH/PEB blend (Figure 8) is obtained from the diffuse light-scattering technique, which we believe to be the most sensitive measurement in the current study. The transition temperatures determined from light transmission and H_v scattering are used as a consistency check, with any discrepancy among the different methods limited mostly to within a 3 °C span around the values determined by the diffuse light scattering. The solid circles are measured data points and the binodal (heavy solid) and spinodal (dashed) curves are calculated from the Flory–Huggins theory for binary polymer mixtures. The existence of LLPS has been confirmed in situ recently using phase-contrast optical microscopy.²⁶ The equilibrium melting temperature in the PEH-rich single phase decreases from 140 \pm 3 °C for pure PEH to 130 \pm 2 °C for H80

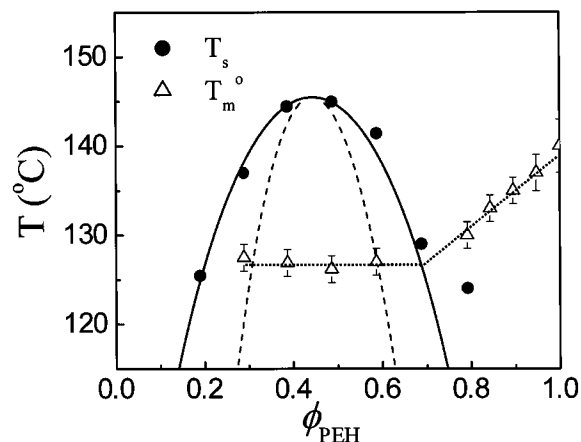


Figure 8. Phase diagram of the PEH/PEB blend. The circles indicate the measured liquid–liquid phase separation temperatures. The solid and dashed curves represent the predicted binodal and spinodal based on the Flory–Huggins formalism with $\chi(T) = -0.0011 + 1.0/T$ (K). The open triangles are equilibrium melting temperatures, which decrease with increasing PEB concentration in the one-phase regime and remain constant in two-phase regime. The dotted lines are guides to the eye.

before intersecting the LLPS boundary. In the two-phase regime, T_m^0 is relatively constant at 127 \pm 2 °C. The dotted lines are guides to the eye; their discontinuity at the LLPS boundary provides additional support for the accuracy of the measurements.

According to the Flory–Huggins theory of polymer blends, the free energy of mixing for two polymers is

$$\frac{\Delta G}{kT} = \frac{\phi_1 \ln \phi_1}{N_1} + \frac{\phi_2 \ln \phi_2}{N_2} + \chi \phi_1 \phi_2, \quad (1)$$

where N_1 and N_2 are the degrees of polymerization (based on a reference volume of four carbon units according to previous studies),^{13–15} and ϕ_1 and ϕ_2 are the volume fractions for the two polymers, respectively. Although this formalism was originally developed for binary mixtures of monodisperse homopolymers, it has been demonstrated experimentally that a moderate polydispersity of 2 as in most metallocene catalyst based polymers does not alter the results.²¹ The interaction parameter, χ , obtained from the fit shown in Figure 8, is $\chi(T) = -0.0011 + 1.0/T$ (K).

Interactions between polyolefins have been extensively studied for hydrogenated model polybutadienes with different side chain content.^{13–15} In that notation, the branching content, denoted as y , indicates the molar fraction of the 1,2-addition butadiene. The interaction

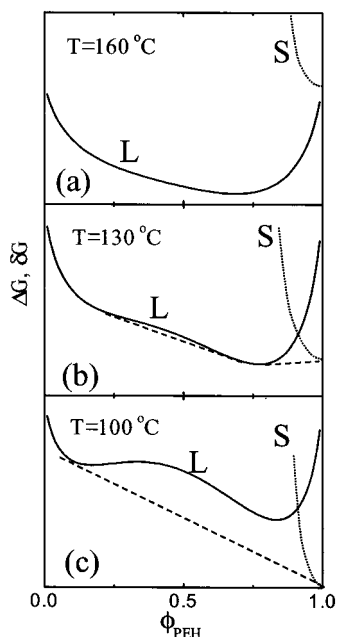


Figure 9. Schematic illustration of the free energy landscape for coexisting liquid–liquid phase separation and crystallization at different temperatures: (a) 160, (b) 130, and (c) 100 °C.

parameter χ increases with increasing branching density difference between polymers 1 and 2, $\Delta y = |y_1 - y_2|$, as well as with increasing overall branching density of the polymers, $\bar{y} = (y_1 + y_2)/2$. In this study, the SCD in units of per 10^3 backbone carbon atoms in Table 1 can be converted to y : $y_{\text{PEH}} = 0.04$ and $y_{\text{PEB}} = 0.26$. In a previous study,¹⁵ the pair with the closest match of both Δy and \bar{y} is a blend with $y_1 = 0$ and $y_2 = 0.25$ that gives $\chi(440 \text{ K}) = 0.0015$. This is in good agreement with the value of 0.0012 suggested by our fit at the same temperature. It would be desirable to compare with SANS measurement on mixtures of hydrogenated and deuterated metallocene-derived copolymers; however, the latter are not presently practical. An extensive previous SANS study on melt interactions between hydrogenated metallocene copolymers with deuterated model polymers shows that their interactions are essentially the same as between model polymers.²¹ That conclusion is reconfirmed in this study by comparing our results to model polymer mixtures, supporting the general understanding that interactions in short-chain branched polyolefin blends are controlled mostly by the branching density, while being less sensitive to other polymer characteristics such as the branch length and polydispersity.

In addition to LLPS, crystallization is important in constructing a complete phase diagram. It would be insightful to construct a unified free energy that describes both crystallization and phase separation. Here we give a schematic discussion of coexisting LLPS and crystallization in light of the phase diagram shown in Figure 8. The additional free energy associated with crystallization, $\delta G(\phi, T)$, decreases monotonically with both temperature and composition of the crystallizable component. Figure 9 shows free energy landscapes for coexisting LLPS and crystallization, where the free energy for the liquid mixture is calculated based on eq 1. The free energy curves as a function of PEH volume fraction for the liquid phase (solid curve, denoted as “L”) and the solid phase (dotted curve, denoted as “S”) are

shown for the temperatures (a) 160, (b) 130, and (c) 100 °C. At 160 °C, minimization of the free energy stabilizes a single liquid phase at any composition. At 130 °C, below both the critical LLPS temperature and the equilibrium melting temperature of the pure PEH, a single liquid phase is stable at low PEH volume fractions. At intermediate PEH concentration, two liquid phases coexist, whereas at higher PEH concentration, a PEH-rich liquid phase coexists with crystalline PEH. Theoretically, a single liquid phase can exist over a very narrow concentration range around the global minimum, however this effect cannot be readily observed in polymers because of molecular weight heterogeneity. At 100 °C, the solid-phase becomes the global minimum, and the crystal coexists with a liquid at most compositions. This phase structure is similar to that of a polystyrene/poly(ϵ -caprolactone) blend reported by Tanaka and Nish.²⁷

In Figure 8, the melting temperature depression at high PEH concentration indicates a single liquid phase right above the equilibrium melting temperature line. If, instead, the crystalline phase is right below the two-phase region, T_m^0 should be constant (as shown in Figure 8) since only the coexisting PEH phase is involved. This observation also holds true for blends with a lower critical solution temperature, as reported by Briber and Khoury.²⁸ An estimate of the interaction parameter from the melting temperature depression has been proposed by Wang and Nish²⁹ and applied to several systems.^{28,30} It is believed that since a negative χ value is always predicted, this approach is likely only applicable to blends with specific interactions.^{28,30}

Metastability plays an important role in polymer phase transitions.³¹ A polymer melt can be supercooled well below the equilibrium melting temperature with limited crystallization, and liquid–liquid phase separation can thus precede crystallization. As shown in Figure 9c, the free energy landscape permits a blend at the critical composition to decompose spontaneously into coexisting liquid phases rather than transform directly to a lower energy crystal state, which is separated from the liquid phase by an energy barrier. In such a scenario, the liquid metastable phase wins. For liquid–liquid phase separation that occurs via nucleation and growth, kinetic competition depends on the relative barrier height for each process. Metastability is thus primarily responsible for observations of liquid–liquid phase separation well below the equilibrium melting temperature.^{32–35}

Further complication comes from the characteristics of the statistical copolymers, pointing toward the meaningfulness of the liquid–liquid phase boundary. The phase boundary is typically measured by two methods; scanning temperature at fixed composition, such as SANS and cloud point measurements, or through measuring the equilibrium coexisting compositions of a phase-separated blend at fixed temperatures, such as diffusion couple, glass transition shift, refractive index measurements, etc. For most homopolymers and truly random copolymers, these two approaches are identical. In copolymer blends with relatively broad polydispersity and short side-chain branching distributions, it is generally believed that the difference in the short side-chain density causes incompatibility so that phase separation represents segregation of the lightly branched and highly branched chains. Such coexisting phases are unlikely to be prepared by mixing certain amounts of

two polymers because of the microstructure distribution differences in pure polymers and in the coexisting phases. Therefore, the phase separation boundary would not be the same when measured with temperature-scan and coexisting composition measurements. However, there is no ambiguity for the critical point. In blends of more heterogeneous polymers, criticality does not exist,³ and simple Flory–Huggins formalism does not apply. This effect may be related to the unusual phase diagram reported for blends of PE and lightly branched PE.^{9–11}

Conclusion

The phase diagram of coexisting liquid–liquid phase separation (LLPS) and crystallization in a blend of statistical ethylene/hexane and ethylene/butene copolymers has been investigated. A variety of techniques, such as diffuse and small-angle light scattering, light transmission, atomic force microscopy, and differential scanning calorimetry, are used to characterize the crystallization-induced contrast and identify the LLPS boundary. An upper critical solution temperature of 146 °C has been revealed in the molten state. The composition dependence of the LLPS boundary follows the prediction of Flory–Huggins theory for binary polymer mixtures, with the interaction parameter, $\chi(T) = -0.0011 + 1.0/T$ (K), based on a reference unit of 4 carbon atoms. Differing from previous studies on LLPS, this approach utilizes the degree of interference between the crystal morphology and LLPS to quantify the phase boundary and can be useful for identifying LLPS boundaries in isorefractive polymer blends where one component is predominantly crystallizable. In practice, only one characterization method need be employed. In the current study, the diffuse light scattering provides the best sensitivity for identifying LLPS boundary. The equilibrium melting temperature of the blends decreases with increasing PEB concentration in the miscible phase, whereas it remains relatively constant at 127 °C within the LLPS coexistence region. The overall phase diagram with coexisting LLPS and crystallization depends on the relative position of the individual transition in the parameter space of composition and temperature. The definition and measurement of the LLPS boundary can be further complicated by polymer microstructure inhomogeneity.

Acknowledgment. We acknowledge Dr. David J. Lohse (ExxonMobil) for providing the polymers for this study, and Drs. Freddy A. Khoury (NIST) and Stephen Z. D. Cheng (Akron) for valuable discussions and advice. B.S.H. acknowledges support from the NSF (DMR 0098104) and ExxonMobil Co.

References and Notes

- (1) Paul, D. R.; Bucknall, C. B. *Polymer Blends*; John Wiley and Sons: New York, 2000.
- (2) Utracki, L. A. *Polymer Alloys and Blends*; Hanser Publishers: New York, 1989.

- (3) Crist, B.; Hill, M. J. *J. Polym. Sci.: Polym. Phys.* **1997**, *35*, 2329.
- (4) Mandelkern, L.; Alamo, R. G.; Wignall, G. D.; Stehlin, E. C. *Trends Polym. Sci.* **1996**, *4*, 377.
- (5) Mirabella, F. M.; Westphal, S. P.; Fernando, P. L.; Ford, E. A.; Williams, J. G. *J. Polym. Sci.: Polym. Phys.* **1988**, *26*, 1995.
- (6) Deblieck, R. A. C.; Mathot, V. B. F. *J. Mater. Sci. Lett.* **1988**, *12*, 1276.
- (7) Rhee, J. W.; Crist, B. *Macromolecules* **1991**, *24*, 5663.
- (8) Barham, P. J.; Hill, M. J.; Keller, A.; Rosney, C. C. A. *J. Mater. Sci. Lett.* **1988**, *7*, 1271.
- (9) Hill, M. J.; Barham, P. J.; Keller, A.; Rosney, C. C. A. *Polymer* **1991**, *32*, 1384.
- (10) Hill, M. J.; Barham, P. J. *Polymer* **1992**, *33*, 4099.
- (11) Lohse, D. J. *Polym. Eng. Sci.* **1986**, *26*, 1500.
- (12) Bates, F. S.; Schulz, M. F.; Rosedale, J. H.; Almdal, K. *Macromolecules* **1992**, *25*, 5547.
- (13) Balsara, N. P.; Fetters, L. J.; Hadjichristidis, N.; Lohse, D. J.; Han, C. C.; Graessley, W. W.; Krishnamoorti, R. *Macromolecules* **1992**, *25*, 6137.
- (14) Graessley, W. W.; Krishnamoorti, R.; Balsara, N. P.; Fetters, L. J.; Lohse, D. J.; Schulz, D. N.; Sissano, J. A. *Macromolecules* **1993**, *26*, 1137.
- (15) Graessley, W. W.; Krishnamoorti, R.; Balsara, N. P.; Butera, R. J.; Fetters, L. J.; Lohse, D. J.; Sissano, J. A. *Macromolecules* **1994**, *27*, 3896.
- (16) Rhee, J.; Crist, B. *J. Chem. Phys.* **1993**, *98*, 4174.
- (17) Budkowski, A.; Klein, J.; Eiser, E.; Steiner, U.; Fetters, L. J. *Macromolecules* **1993**, *26*, 3858.
- (18) Scheffold, F.; Eiser, E.; Budkowski, A.; Steiner, U.; Klein, J.; Fetters, L. J. *J. Chem. Phys.* **1996**, *104*, 8786.
- (19) Alamo, R. G.; Londono, J. D.; Mandelkern, L.; Stehling, F. C.; Wignall, G. D. *Macromolecules* **1994**, *27*, 411.
- (20) Wignall, G. D.; Alamo, R. G.; Londono, J. D.; Mandelkern, L.; Stehling, F. C. *Macromolecules* **1996**, *29*, 5332.
- (21) Reichart, G. C.; Graessley, W. W.; Register, R. A.; Lohse, D. J. *Macromolecules* **1998**, *31*, 7886.
- (22) Certain equipment and instrument materials are identified in the paper in order to adequately specify the experimental details. Such identification does not imply recommendation by the National Institute of Standards and Technology, nor does it imply the materials are necessarily the best available for the purpose.
- (23) A detailed description of the temperature gradient hot stage is discussed elsewhere, see: Meredith, J. C.; Karim, A.; Amis, E. J. *Macromolecules* **2000**, *33*, 5760.
- (24) Stein, R. S.; Rhode, M. B. *J. Appl. Phys.* **1960**, *31*, 1873.
- (25) Hoffman, J. D.; Weeks, J. J. *J. Chem. Phys.* **1965**, *42*, 4310.
- (26) Wang, H.; Shimizu, K.; Kim, H. D.; Wang, Z.-G.; Hobbie, E. K.; Han, C. C. *J. Chem. Phys.*, in press.
- (27) Tanaka, H.; Nishi, T. *Phys. Rev. Lett.* **1985**, *55*, 1102; *Phys. Rev. A* **1989**, *39*, 783.
- (28) Briber, R.; Khoury, F. *Polymer* **1987**, *28*, 38; *J. Polym. Sci. Part B, Polym. Phys.* **1993**, *31*, 1253.
- (29) Nish, T.; Wang, T. T. *Macromolecules* **1975**, *8*, 909.
- (30) Jo, W. H.; Park, S. J.; Kwon, I. H. *Polym. Int.* **1992**, *29*, 173.
- (31) Cheng, S. Z. D.; Keller, A. *Annu. Rev. Mater. Sci.* **1998**, *28*, 533.
- (32) Chen, H. L.; Hwang, J. C.; Wang, R. C. *Polymer* **1998**, *39*, 6067.
- (33) Tomuro, H.; Saito, H.; Inouue, T. *Macromolecules* **1992**, *25*, 1611.
- (34) Svoboda, P.; Kressler, J.; Chiba, T.; Inoue, T.; Kammer, H. W. *Macromolecules* **1994**, *27*, 1154.
- (35) Isayeva, I.; Kyu, T.; Manley, R. St. J. *Polymer* **1998**, *39*, 4599.

MA010900F